Simultaneous Effects of a Vortex Generator and Magnetic Field on Ferrofluid Convective Heat Transfer in a 3D Channel: First and Second Law Analyses

Ali Jalayeri, Hossein Soltanipour*, Sajadollah Rezazadeh

Department of Mechanical Engineering, Urmia University of Technology (UUT), Urmia, Iran

ABSTRACT: This article presents a comprehensive approach to enhance heat transfer rates in a 3D channel using Ferrofluids. The study investigates the individual and combined impacts of rectangular winglet vortex generators and magnetic fields on flow characteristics, heat transfer enhancement, and entropy generation. Numerical solutions are derived for the governing partial differential equations using the finite volume technique and the SIMPLE algorithm. The investigation assesses the influence of key parameters, including the type of rectangular winglet vortex generator (simple, concave, and convex), Reynolds number, and magnetic field strength. Optimal operational conditions are identified based on thermodynamics' first and second laws. This study has been conducted in three steps, and the interaction of created vortices and their effect on heat transfer, pressure drop, and entropy production were investigated. In the first step, the effect of the vortex generator in different Reynolds has been investigated. In the next step, the impact of applying a magnetic field at different intensities by a current-carrying wire has been studied in a channel without vortex generators. Finally, the application of vortex generators and magnetic fields has been investigated simultaneously. The results showed that using the concave vortex generator in the absence of a magnetic field increased the heat transfer by 50% and pressure drop by 60%. Applying a magnetic field in the channel without vortex generators has increased heat transfer and pressure drop by 70% and 118%, respectively. Moreover, it is observed that the magnetic field induces a greater pressure drop penalty than the vortex generator for achieving the same heat transfer augmentation. The simultaneous application of magnetic field and vortex generator has also increased the heat transfer and pressure drop by 200% and 269%, respectively, for simple vortex generators.

1- Introduction

Right now, based on the needs of the energy industry, such as oil, gas, and petrochemicals, one of the foremost vital components in keeping up the well-being of control plants and avoiding harm to turbines and generators is utilizing heat exchangers for cooling. Innovative and efficient methods to enhance heat transfer are crucial for improving and optimizing thermal systems. Generally, such techniques can be categorized as passive, active or a combination of both. Active methods, like ferrohydrodynamic (FHD) and magnetohydrodynamics (MHD), require external forces to manipulate fluid flow and augment the rate of heat transfer [1]. In contrast, passive methods often rely on improving the heat transfer surface geometry or changing the working fluid properties. This is done using roughness elements like ribs and vortex generators (VG) [2-4]. Advances in nanotechnology have greatly improved the thermophysical properties of common liquids over the past twenty years by

utilizing nanoparticles [5]. Current literature indicates that many researchers have used either magnetic fields (MF) or vortex generators to enhance convection. The influence of an MF on Ferrofluid convection in a channel with wavy walls was reported by Mousavi et al. [6]. Their findings showed that raising the MF gradient from 0 to 1.5×10^5 led to a threefold augmentation in the heat transfer rate and an elevenfold increment in the friction coefficient on the top wall. The study conducted by Ibrahim et al. [7] involved analyzing forced convection through a microchannel containing porous blocks and an MF. The results of the study showed that the thermal efficiency index increased by 33% when using MF and by 89% when using both MF and porous blocks at the same time. Gorjaei et al. [8] carried out a numerical investigation on the impacts of Reynolds number and MF on heat transfer augmentation of magnetic nanofluid convection in a tube. It was observed that increasing the MF intensity resulted in a reduction in the entropy production rate. Izadi et al. [9] determined the role of MFs on the cooling performance of a porous CPU filled with nanofluids. Their results showed that increasing the Darcy number increased

*Corresponding author's email: h.soltanipour@gmail.com

the convection speed by increasing the Eckert number, which decreased the Nusselt number. The Nusselt number decreased significantly at low porosity values as the Hartmann number increased. However, for large porosity coefficient values, the opposite effect was observed. A numerical study conducted by Bezatpour et al. [10] investigated how MFs affect Ferro fluid convection in a heat exchanger. They concluded that the convection rate increased with the application of MF and that MF was more effective at low Reynolds numbers. Ali et al. have conducted a study on a vertical duct under the influence of a MF. In this study, they have investigated the effect of the field on the flow structure and the velocity field. Their results showed that in the absence of a MF, the flow is symmetric in the x and y directions, and velocity is maximum at the center of the duct. while symmetry is distorted with a strengthened MF, and flow becomes to slow down gradually [11]. An experimental analysis of the convection of magnetic fluid in a horizontal pipe under the impact of MF was performed by Sun et al. [12]. Their results demonstrated that augmentation of the intensity and gradient of MF significantly enhanced the convective heat transfer rate and flow losses. Generally, the heat transfer increment prevailed over the pressure drop. With an MF gradient of 28.6 and magnitudes of 415 and 700G, the Nusselt number increased by 7.19% and 32%, respectively. The effect of the magnetic field angle on the heat transfer in the porous medium was investigated octagonal cavity with oval barriers by Roshani et al. The results obtained for both cavities and oval barriers show that with the Rayleigh number being constant, the value of the maximum stream function decreases with the increase of the Hartmann number. When the Hartmann number is constant, with increasing Rayleigh number, its value increases significantly. Also, In both cavities, if the Hartmann number is constant, in all the angles of the magnetic field effect, as the Rayleigh number increases, the value of the average Nusselt number decreases [13]. A numerical analysis performed by Mehrez et al. [14] illustrated the impact of MF on the Ferrofluid convection inside a two-dimensional channel. Their qualitative results showed significant changes in the temperature field and streamlines under the impact of MF. The generation of a secondary flow near the MF source destroyed the temperature boundary layer, causing an increase in the convective heat transfer rate. Selimefendigil et al. [15] explored the influence of local wall curvature and MF on forced convection of water-based CNT nanofluids at $100 \leq Re \leq 400$. They found that adding curvature to the wall significantly affected fluid flow behavior and heat transfer rates. In addition, the used MF improved the heat transfer rate by 22.48%. Soltanipour [16] analyzed the forced convection of a magnetic fluid in an annulus under the action of MF using a two-phase approach. The numerical results indicated that each current-carrying wire creates four vortices across the cross-section. It was indicated that the maximum heat transfer augmentation is achieved with a three-wire configuration at all MF strengths. Using vortex generators (VG) on the heat transfer surface creates eddies that destroy the thermal boundary layer, promote fluid mixing, and increase the convection heat transfer rate. Therefore, rough elements of various shapes find wide applications in thermal systems such as heat exchangers. Different researchers have investigated various parameters, including VG shape [17, 18], angle of attack [19], and VG configuration [20]. Ke et al. [21] investigated the impact of triangular VG arrangements (convergent, divergent, and compound) on pressure drop and heat transfer rate. They recognized that both channel tallness and VG perspective proportion are persuasive parameters. Their discoveries appeared that the compound course of action caused more noteworthy blending and expanded the great exchange coefficient when the channel tallness was low. Moreover, expanding the VG height-to-length ratio proportion in all three arrangements moved forward the significant exchange in heat transfer coefficient. Amini et al. An analysis of nanofluid heat transfer in a channel with six rotating rectangular VGs was conducted by [22]. They examined the impacts of Reynolds number, rotational velocity, and direction of rotation on the heat transfer rate and pumping power. Pressure drop and heat transfer were higher when VGs rotated concurrently rather than oppositely.

Heydari et al. have worked on optimizing heat transfer using micro pin-fins and microVGs. Their study combines two concepts of micro pin-fins and micro vortex generators to enhance heat transfer and mixing, with the aim of improving the overall performance of the heat transfer system. The results indicate that combining a micro vortex generator and a micro pin-fin would improve the system's overall performance when compared to the performance of both components separately [23]. Asadi et al. [24] reported on the impact of longitudinal VGs on heat transfer and pressure drop. They employed three different VGs in two distinct layouts: Common Flow Down (CFD) and Common Flow Up (CFU). Their findings revealed higher heat transfer and pressure drop in the CFU configuration than for all VGs. Lemend et al. [25] assessed the influence of a trapezoidal VG on the convection rate and flow characteristics. Their results demonstrated that this type of VG induces three pairs of corner vortices and one pair of main vortices in the cross-section. This leads to enhanced fluid mixing and better heat transfer performance. Zhen et al. have researched the enhancement of heat transfer performance caused by vortex generators in novel airfoil channels. The results show that the VG improves the synergistic effect of the velocity field and temperature gradient field, leading to the increase of turbulent kinetic energy and a decrease of heat transfer entropy production in the channel, which finally promotes the enhancement of heat transfer [26].

One of the most essential components of the oil, gas, and petrochemical industries is using heat exchangers. These heat exchangers are usually used to cool the working fluid flow. One of the most economical types of heat exchangers is their plate type. In previous studies, different effects, such as vortex generator and magnetic field, have been investigated separately regarding heat transfer and pressure drop. Considering that both the vortex generator and the magnetic field are among the methods of creating the vortex in the flow, the innovation of the present study can be examined from two aspects. One is due to considering the simultaneous effect of

vortex generator and magnetic field on heat transfer and flow pattern, and the other is due to solving the problem based on the second law of thermodynamics in terms of entropy production. This study first examines the effect of simple, concave, and convex vortex generators in different Reynolds numbers. The next step investigates the effect of different magnetic fields in the channel without the vortex generator. Finally, according to the results, the simultaneous effect of the vortex generator and the magnetic field is investigated in terms of thermodynamics' first and second laws.

2- Problem Definition

Fig. 1 shows a 3D channel that contains a pair of rectangular winglet VGs on the bottom wall. In this work, three types of VGs are employed: simple, convex, and concave. The curved VGs have a curvature angle of β= 60°, while for all VGs, the angle of attack is set to α=45°. A current-carrying wire is located underneath the bottom wall along the Z-axis. The bottom wall is heated with a uniform and constant heat flux q'', while the top wall is insulated. In the present investigation, a single-phase model is used to evaluate the effects of MFs on the Fe_3O_4/Water ferrofluid forced convection. The volume fraction of nanoparticles is taken to be 2%. Details regarding the channel, VG, and wire geometries are listed in Table 1.

3- Calculation of MF intensity, magnetization, and ferrofluid thermos physical properties

The components and magnitude of the MF intensity caused by a single current-carrying wire located at (x_w, y_w) can be obtained from the following equations[27]:

$$H_x = \frac{I}{2\pi} \frac{(y-y_w)}{[(x-x_w)^2+(y-y_w)^2]} \tag{1}$$

$$H_y = \frac{-I}{2\pi} \frac{(x-x_w)}{[(x-x_w)^2+(y-y_w)^2]} \tag{2}$$

$$H(x,y) = \sqrt{H_x^2 + H_y^2} \tag{3}$$

The following equations are used to calculate the magnetization of the ferrofluid[28]:

$$M = M_s L(\xi) \tag{4}$$

$$M_s = \varphi m_d \tag{5}$$

$$L(\xi) = \text{Coth}(\xi) - \frac{1}{\xi} \tag{6}$$

$$\xi = \frac{\mu_0 m_d \forall_p H}{k_B T} \tag{7}$$

In the above equations, $m_d = 446 \times 10^3$ A/m (the domain magnetization of the Fe_3O_4 particle) and $k_B = 1.380649 \times 10^{-23}$ J/K (the Boltzmann coefficient). Moreover, M_s is saturation magnetization, $L(\xi)$ is Langevin equation, ξ is Langevin parameter, μ_0 is the permeability of the vacuum, T is temperature and $\forall_p = \delta d_{np}^3/6$ is the volume of a single particle[29].

The density and heat capacity of the ferrofluid are determined by Equations 8 and 9[30, 31].

$$\rho_{ff} = \varphi \rho_p + (1-\varphi)\rho_{bf} \tag{8}$$

$$(\rho c_p)_{ff} = \varphi(\rho c_p)_p + (1-\varphi)(\rho c_p)_{bf} \tag{9}$$

In the above equations, p, bf, and ff refer to particles, base liquid, and ferrofluid.

The dynamics viscosity (μ_{ff}) and conductivity (k_{ff}) of ferrofluid are functions of magnetic flux, temperature, and volume fraction obtained from equations 10 and 11[32, 33].

$$\mu_{ff} = 0.001 \exp((-0.02(T+273.15)) \\ \times (0.00035B^2 + 0.31B - 27886.48\varphi^2 \\ + 4263.02\varphi + 316.06)) \tag{10}$$

$$k_{ff} = \left[1 + 0.58\varphi^{0.6158}\left(\frac{10^4 B}{B_{min}}\right)^{1.02}\right] \\ \times \left[1 + \varphi + 119.22\varphi\left(\frac{T}{T_{min}}\right)^{0.06423}\right]k_{bf} \tag{11}$$

In the above equations, T and B are temperature (in Celsius) and magnetic flux (in Gauss). Moreover, $B_{min} = 100$ G and $T_{min} = 20°C$. Finally, the base liquid thermal conductivity is determined from:

$$k_{bf} = (-6.58 \times 10^{-6} T^2 + 0.0018 T + 0.5694) \tag{12}$$

The thermophysical properties of the carrier liquid and nanoparticles are summarized in Table 2.
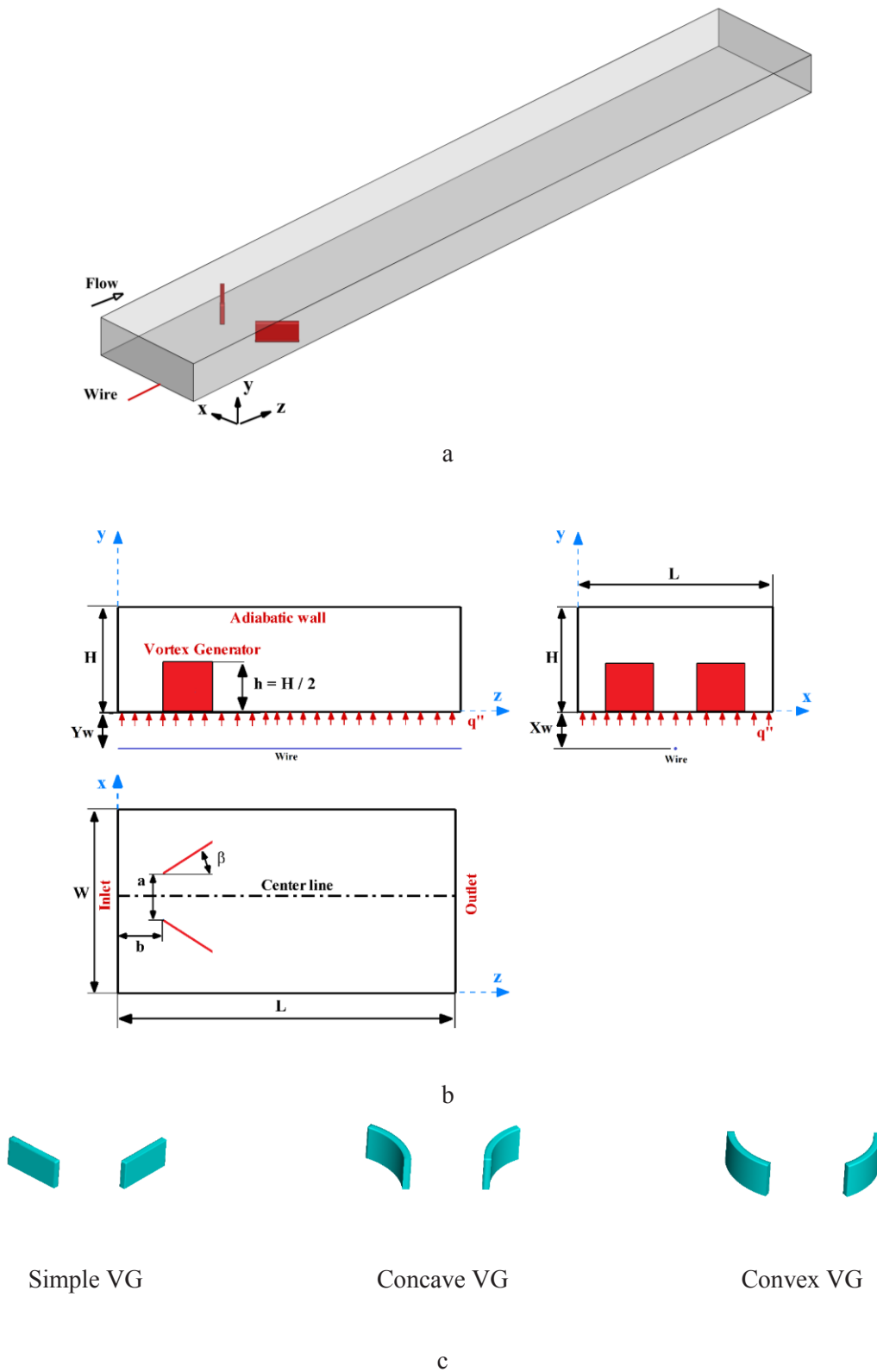
a

b

Simple VG   Concave VG   Convex VG

c

Fig. 1. The geometry of the channel, VGs, and wire a) 3D view of the geometry b) Y-Z plane, X-Z plane, X-Y plane, c) VG types.

Table 1. Geometrical details of the channel, VG, and wire

Channel		Vortex Generator				Wire	
H	4mm	l/H	1	a/H	1	X_w /H	1.5
W/H	3	t/H	0.1	b/H	3	Y_w /H	-0.25
L/H	20	h/H	0.5				

Table 2. Thermophysical properties of the base fluid and nanoparticles [34, 35]

Phase	ρ [kg/m^3]	k [W/m.K]	c [J/kg.K]	μ [kg/m.s]$\times 10^{-6}$	dp [nm]
Particles	5180	80.4	670	-	25
Base Fluid	997.1	k_{bf}	4197	855	-

4- Nondimensionalized governing equations and boundary conditions

The governing equations have been made dimensionless using the following set of dimensionless parameters to generalize the numerical results[16, 36]:

$$\nabla^* = D_h \nabla, \quad p^* = \frac{p D_h^2}{\rho_{bf} \alpha_{bf}^2}, \quad V^* = \frac{V D_h}{\alpha_{bf}}$$

$$T^* = \frac{(T\text{-}T_{in}) k_{bf}}{(q_w^* D_h)}, \quad M^* = \frac{M}{M_0}, \quad H^* = \frac{H}{H_0},$$

$$Re = \frac{\rho_{bf} V_{in} D_h}{\mu_{bf}} \quad Ec = \frac{k_{bf} \mu_{bf}^2}{D_h^3 \rho_{bf}^2 C_{P,bf} q^*},$$

$$q^* = \frac{q_w^* D_h}{(k_{bf} T_{in})}, \quad Mn = \frac{(\mu_0 H_0 M_0 D_h^2)}{(\rho_{bf} \alpha_{bf}^2)}, \quad Pr = \frac{\upsilon_{bf}}{\alpha_{bf}}$$

The non-dimensional parameters used to generalize the numerical results include the non-dimensional gradient operator, pressure, velocity, temperature, magnetization, MF intensity, Reynolds and Eckert numbers, heat flux, magnetic number, and Prandtl number denoted by where ∇^*, p*, V*, T*, M*, H*, Ec, q*, Mn and Pr, respectively. It should be noted that in the present study, the hydraulic diameter is considered to be $D_h = 2H$.

Also, H_0 and M_0 are calculated from Eqs. (13) and (14).

$$H_0 = H(\frac{3H}{2}, 0) \tag{13}$$

$$M_0 = M(H_0, T_{in}) \tag{14}$$

In dimensionless form, continuity, momentum, and energy equations are given as follows:

continuity

$$\nabla^* . V^* = 0 \tag{15}$$

momentum

$$\frac{\rho_{ff}}{\rho_{bf}} \nabla^* . (V^* V^*) =$$
$$-\nabla^* p^* + Pr \nabla^* . \left[\left(\mu_{ff} \middle/ \mu_{bf} \right) \nabla^* V^* \right] \tag{16}$$
$$+ Mn M^* \nabla^* H^*$$

energy

$$\frac{(\rho c_p)_{ff}}{(\rho c_p)_{bf}} V^* . \nabla^* T^* =$$
$$\nabla^* . \left(\left(\frac{k_{ff}}{k_{bf}} \right) \nabla^* (T^*) \right) + \frac{\mu_{ff}}{\mu_{bf}} \left(\frac{Ec}{Pr} \right) \phi_v^* \tag{17}$$

Table 3 presents the boundary conditions in dimensionless

Table 3. Non-dimensional boundary conditions

Boundary	Type of Boundary	Mathematical Expression
Inlet	Uniform Velocity and Temperature	$u^* = v^* = 0$; $w^* = RePr$; $T^* = 0$
Upper Wall	No Slip - Adiabatic	$u^* = v^* = w^* = 0$; $q^* = 0$
Bottom Wall	No Slip – Constant Heat Flux	$u^* = v^* = w^* = 0$; $\partial T^*/\partial y^* = - k_{bf}/k_{ff}$
Side Walls	Symmetry	$\partial \psi^*/\partial x^* = 0$; $\psi^* = u^*, v^*, w^*, T^*, P^*$
Outlet	Zero gradient	$\partial u^*/\partial z^* = \partial v^*/\partial z^* = \partial w^*/\partial z^* = \partial^2 T^*/\partial z^{*2} = 0$

form.

The local Nusselt number is calculated from Eq.18 which $T^*_w(z^*)$ is the non-dimensional wall temperature and $T^*_m(z^*)$ is the mean temperature of the ferrofluid.

$$Nu(z^*) = \frac{1}{T^*_w(z^*) - T^*_m(z^*)} \tag{18}$$

$$T^*_m(z^*) = \frac{\iint u^* T^* dx^* dy^*}{\iint u^* dx^* dy^*} \tag{19}$$

Equation (20) yields the average Nusselt number:

$$Nu = \frac{1}{10} \int_0^{10} Nu(z^*) \, dz^* \tag{20}$$

The pressure drop coefficient and thermal performance coefficient can be determined from Eqs. (21) and (26)[37].

$$f = \frac{P^*_{in} - P^*_{out}}{5(RePr)^2} \tag{21}$$

$$PEC = \left(Nu \big/ Nu_0 \right) \Big/ \left(f \big/ f_0 \right)^{1/3} \tag{22}$$

A parameter called the secondary flow intensity is usually used to measure the strength of the secondary flow and is calculated as follows [28].

$$I_{sec} = \frac{\sqrt{(u^*)^2 + (v^*)^2}}{RePr} \tag{23}$$

5- Calculation of entropy generation rate

The performance of thermal systems is always degraded due to irreversibility. From a thermodynamics point of view, the entropy production rate is a quantitative criterion for the degree of irreversibilities in a thermal system. Heat transfer and fluid friction are primarily responsible for irreversibilities in convection problems. The dimensionless local entropy generation due to friction ($S^{''}_f$), heat transfer ($S^{''}_T$), and total entropy generation ($S^{''}_{gen}$) are given by[38-40]:

Thermal entropy generation

$$S^{''}_T = \left(\frac{k_{ff}}{k_{bf}} \right) \frac{\left| \nabla^* T^* \right|^2}{\left(T^* + \frac{1}{q^*} \right)^2} \tag{24}$$

Frictional entropy generation

$$S^{''}_f = \left(\mu_{ff} \big/ \mu_{bf} \right) Ec.Pr \frac{\phi^*_v}{\left(T^* + \frac{1}{q^*} \right)} \tag{25}$$

Table 4. Grid independence for the channel with simple VG at Re=1000, $\alpha=45^O$ and Mn=1.5×10^{10}

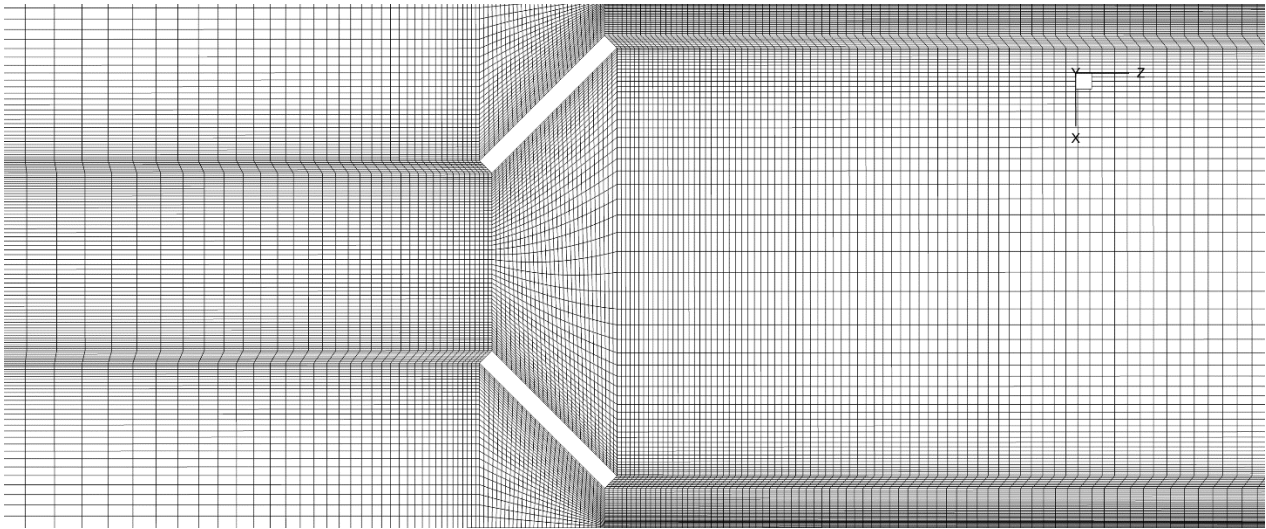| Mesh no.	Cells no.	Nu	Error%	f	Error%
1	700000	61.362	-	0.557	-
2	900000	59.757	2.615	0.546	1.975
3	1150000	59.026	1.223	0.539	1.282
4	1300000	58.527	0.845	0.537	0.529
5	1450000	57.999	0.028	0.535	0.372

Fig. 2. Structural grid for the channel with simple VG

Total entropy generation

$$S_{gen}^{''} = S_f^{''} + S_T^{''} \qquad (26)$$

Finally, the non-dimensional entropy generation is obtained by integration over the entire computational domain[41]:

$$S_i^* = \int_0^{10} \int_0^{0.5} \int_0^{1.5} S_i^{''} dx^* dy^* dz^*; \quad i=T,f, gen \qquad (27)$$

6- Numerical method and grid study

The well-known finite volume approach method is utilized for the solution of the governing equations. Central difference and second-order upwind schemes are employed to discretize diffusion and advection terms. The pressure and velocity fields are coupled via the SIMPLE algorithm. Gauss-Seidel (a point implicit), along with an algebraic multigrid approach, is used to solve linear discretized equations. The solution is deemed to have converged when the scaled residuals for all equations are less than a specified threshold of 10^{-7} [42].

Five structured grids were tested to confirm grid independence. The mean Nusselt number and pressure drop coefficient were compared in Table 4, indicating that as the cell count increases from 1300000 to 1450000, the relative error for both the Nusselt number and pressure drop factor is less than 1%. Hence, mesh four was used for all scenarios. Fig. 2 shows the mesh topology.

7- Validation

To verify the numerical results, the present study was carefully compared with similar published studies in the literature. First, the local Nusselt number variation was compared with the experimental data of Asfer et al.[43] and
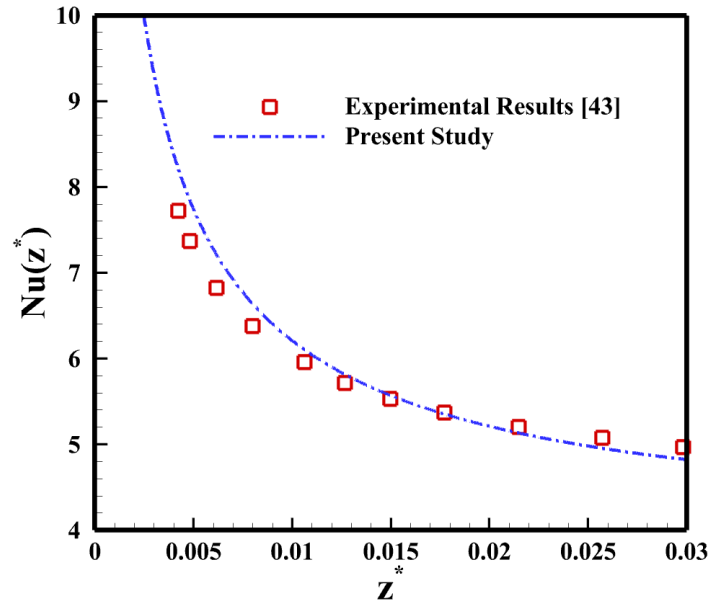
Fig. 3. Compression of the local Nusselt number between numerical and experimental results for Pe = 2496 and φ=0.05
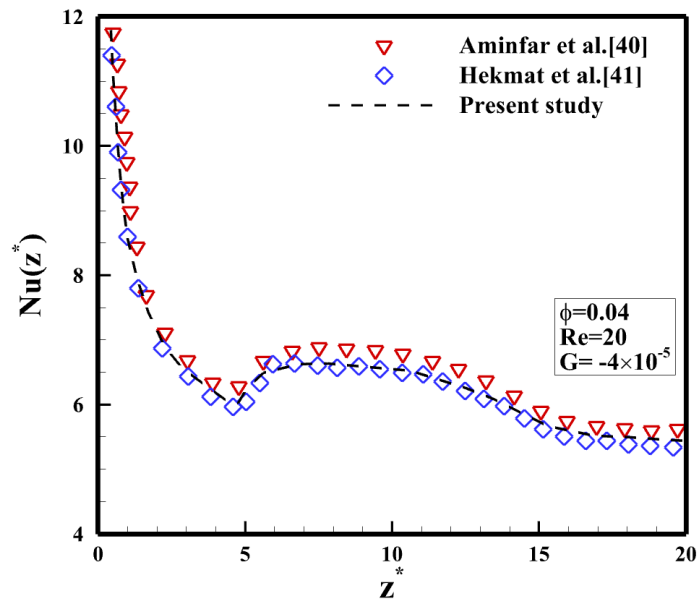

Fig. 4. Local Nusselt number validation versus the results presented in Ref. 43 and 44

present numerical results for ferrofluid heat transfer in a pipe. As depicted in Fig. 3, the average error is 3%, indicating reasonable agreement between the results.

In the next step, another comparison was made with numerical results of [44] and [45] for mixed convective magnetic liquid in a vertical annulus under a linear MF. As seen in Fig. 4, there is acceptable consistency between the current study and the results of references 40 and 41.

The next step involves comparing the present numerical results with experimental data on fluid flow in a channel containing a pair of rectangular VGs (a=45°). Table 5 presents the comparison, which confirms the excellent agreement between the results.

In the final validation, the Nusselt number variation along the channel (which contained a pair of rectangular VGs with an angle of attack of 90°) was compared to Abdullahi and Shams' numerical results [47]. As illustrated in Fig. 5, the results of the current investigation are in good accordance

Table 5. Comparison of the Nusselt number in a channel with rectangular VG with the experimental study [46]

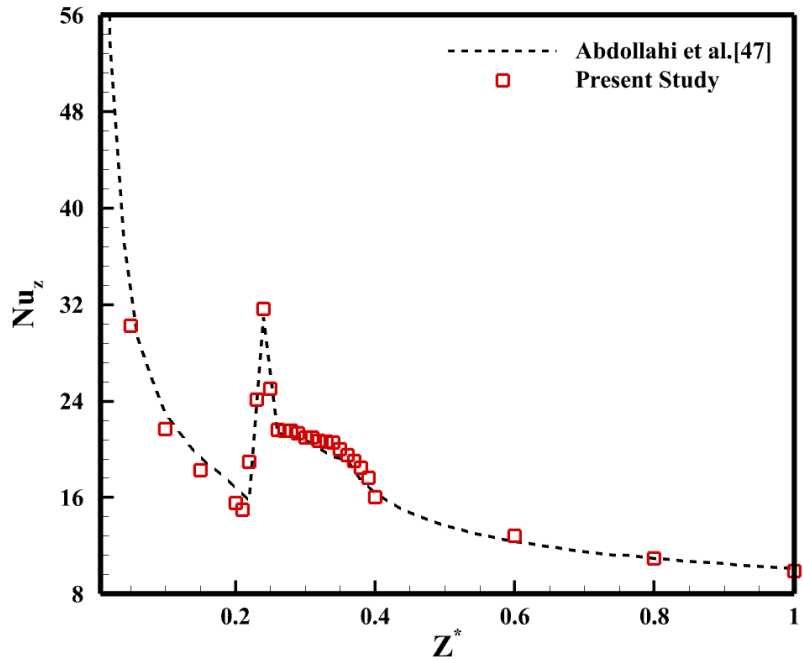|	J/J_0		
Re	Numerical	Experimental	Error (%)
700	1.006	0.99	1.62
1300	1.121	1.110	0.99
2500	1.110	1.100	0.91

Fig. 5. Validation of local Nusselt number for the channel flow with VG at Re=350

with the published data.

8- Results and Discussion

The main objective of the present work was to evaluate the simultaneous effects of MF and VGs upon the ferrofluid convection rate, pressure drop, and entropy production in a rectangular channel. In the following, the impact of Reynolds number (250<Re<1000), magnetic number ($0 < Mn < 10^{10}$), and VG shape (simple, concave, and convex) will be studied.

8- 1- Impact of vortex generator

This section examines how Reynolds number and VG types affect fluid flow patterns, heat transfer, and entropy generation. Fig. 6 displays streamlines, axial velocity, secondary flow intensity, and temperature fields at $Z^*=5$ for Re=1000 and three VG types (Simple, Concave, and Convex). Fig. 6 (a) compares the general flow patterns for all three VGs, showing two pairs of large vortices (main vortices) and a pair of small cells in the lower corner of the cross-section. For the concave and convex VG, the middle vortices are split into two vortices. Fig. 6 (b) presents an axial velocity distribution, indicating high-velocity zones at the middle of the cross-section. The peak values for the axial velocity of simple, concave, and convex VGs are 9600, 9500, and 9300, respectively. Fig. 6 (c) displays secondary flow intensity contours, indicating that the main vortices have
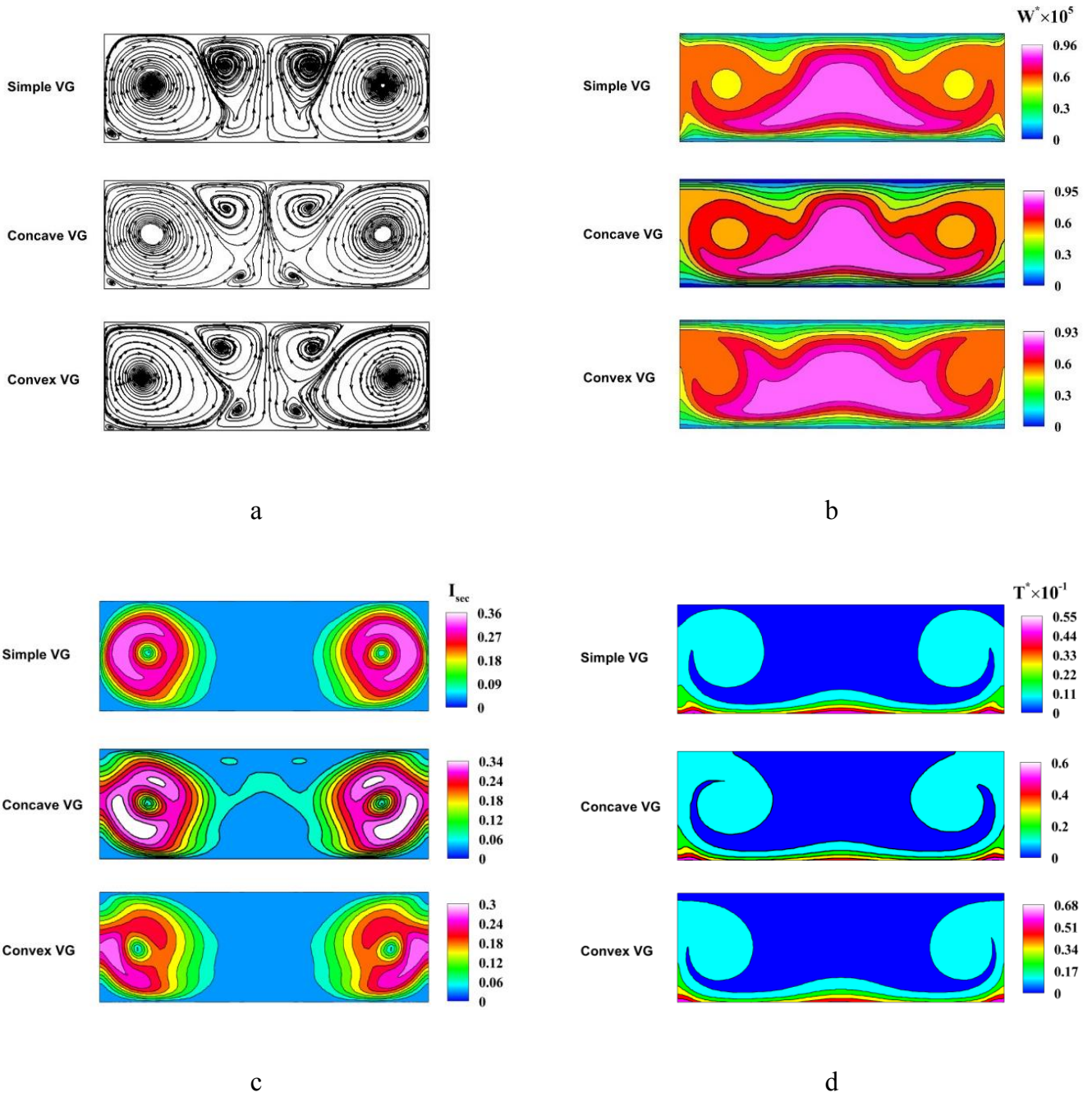
a

b

c

d

Fig. 6. a) streamlines b) axial velocity c) secondary flow intensity d) temperature field at Re=1000 and Mn=0
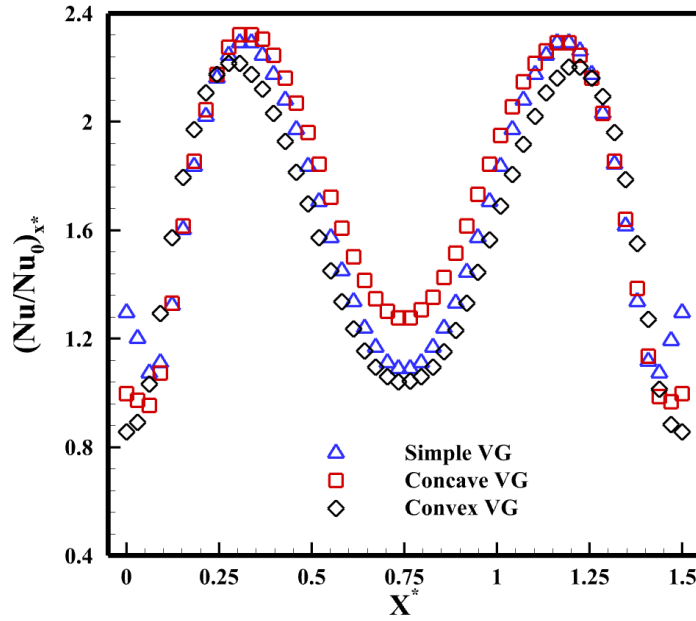
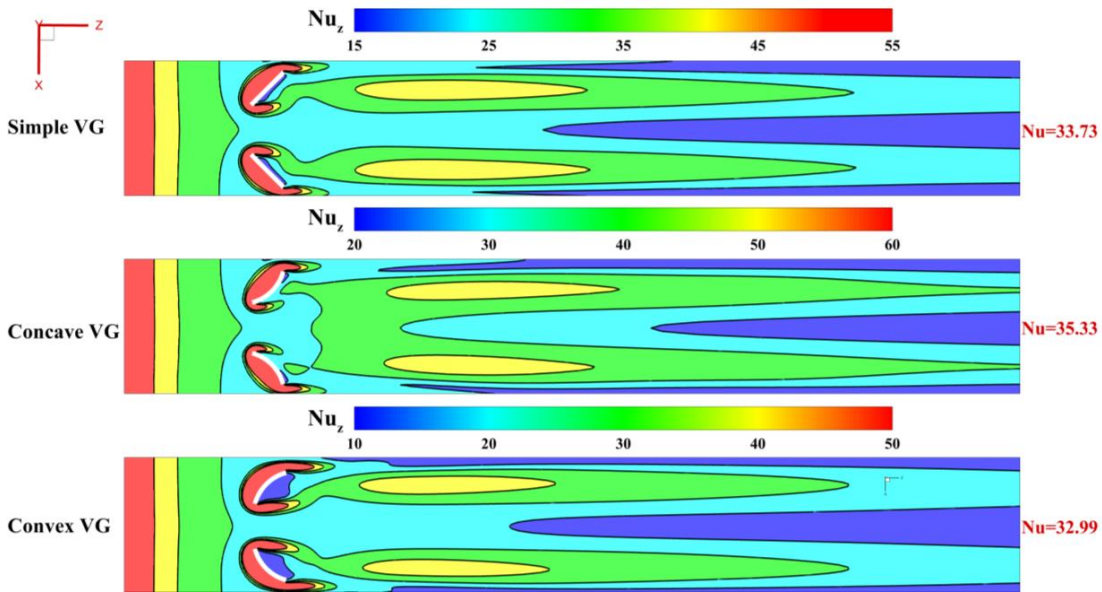**Fig. 7. The local Nusselt number profiles along the X-axis at the , Re=1000 and Mn=0**

Fig. 8. The Nusselt number distribution on the bottom wall for Re=1000 and Mn=0

the highest values of intensity. The secondary flow intensity of the middle and lower corner vortices is negligible. The maximum value of secondary flow intensity at the cross-section for the simple VG is 36%, which means the secondary flow caused by the VG is about 36% of the inlet velocity. Fig. 6 (d) exhibits that the cross-sectional distribution of the temperature is nearly identical for all three VGs. As one moves from the center of the cross-section to the sidewalls, the thickness of the thermal boundary layer decreases, and

fluid mixing becomes more apparent.

Fig.7 displays the spanwise profile of the Nusselt number at $Z^*=5$. There are two maxima and one minimum in each curve, whose location is influenced by the direction of the secondary flow vector. The channel with a concave VG has a higher average Nusselt number than the channels with simple and convex VGs.

Fig. 8 compares the Nusselt number distribution on the bottom wall (heated wall) at Re=1000 for the three VGs. The
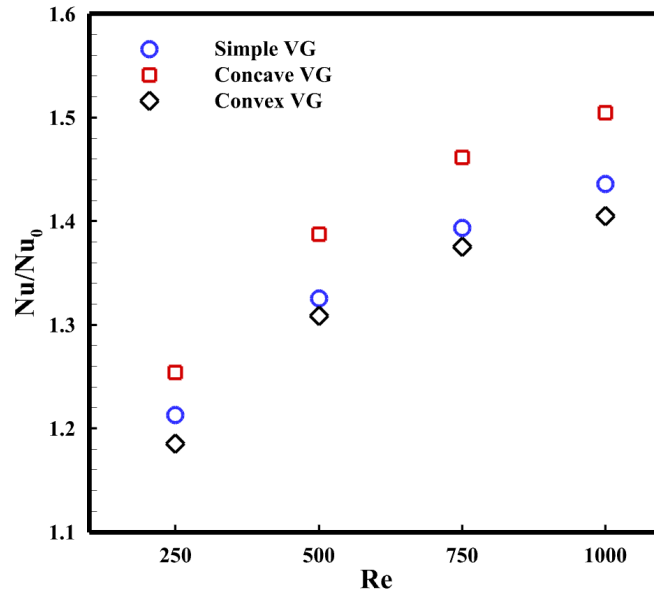
(a)
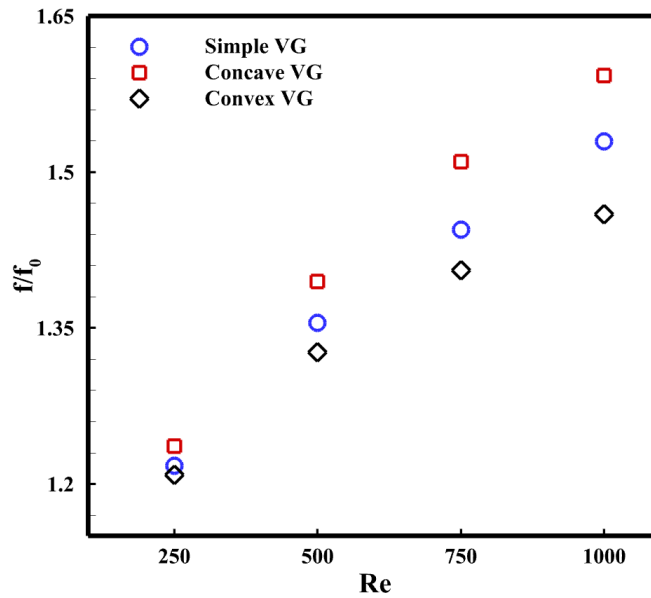
(b)

Fig. 9. The variation of a) average Nusselt number, b) pressure drop coefficient, and c) thermal performance coefficient at Mn=0 (Continued)

Nusselt distribution before the VG is the same for all three VGs. After the flow passes over the VG, the Nusselt number increases significantly. However, flow separation after the VG creates a low-pressure region and reduces the rate of heat transfer. The convex VG widens the wake area, leading to a lower Nusselt number. The high Nusselt number zone (green zone) is associated with the main vortex, while the low Nusselt number zone (blue zone) is associated with the middle and bottom corner eddies.

Fig. 9 displays the influence of Reynolds number and VG type on (Nu/Nu_0), (f/f_0), and thermal performance (PEC). According to Fig. 9 (a) and (b), the presence of VGs increases the heat transfer and pressure drop of channels in comparison with those without VGs. Furthermore, the role of VG in the enhancing convection rate is more evident at high Reynolds numbers. Out of the three VGs, the concave VG has higher Nu/Nu_0, f/f_0 and PEC values as depicted in Fig. 9 (c). The maximum heat transfer augmentation, pressure drop
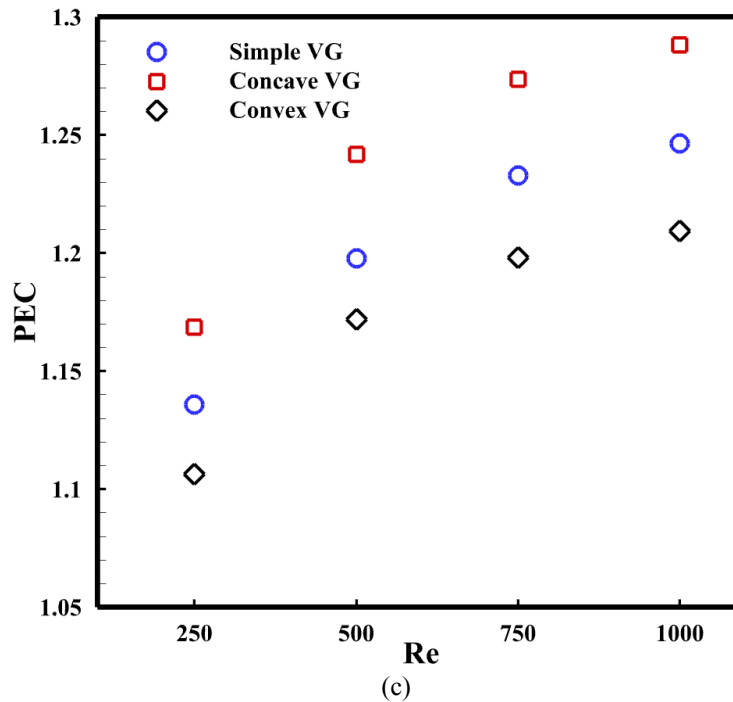
(c)

Fig. 9. The variation of a) average Nusselt number, b) pressure drop coefficient, and c) thermal performance coefficient at Mn=0

coefficient, and PEC values of the concave VG at Re=1000 are 1.504, 1.593, and 1.288, respectively.

Fig. 10 compares the entropy production rates due to thermal, friction, and overall entropy for three types of VGs. As shown, an increase in Reynolds number results in higher frictional entropy production. On the other hand, inducing secondary flows through fluid mixing increases the heat transfer coefficient, which in turn reduces the temperature gradient and mitigates thermal entropy. Fig.10 (a) also demonstrates that, regardless of the Reynolds number, channels with a concave VG exhibit the lowest thermal entropy production and the highest frictional irreversibility. Of the three examined VGs, the concave VG has the lowest overall entropy generation and the best thermal performance in accordance with the second law of thermodynamics, as shown in Fig. 10 (b). In general, the findings suggest that heat transfer-induced entropy plays a predominant role in total irreversibility. The general results obtained from the curves of thermal performance and total entropy production show that the channel with concave VG is associated with the maximum PEC and the minimum total entropy production. Therefore, from the perspectives of the first and second laws, the optimal operating conditions for the channel can be achieved using concave VG.

8- 2- Simultaneous effect of magnetic field and vortex generator

This section presents the simultaneous impacts of VG and MF on the convection heat transfer intensification and entropy production rate at Re=1000. Fig. 11 shows the intensity distribution of MF and X and Y components of the Kelvin body forces at Z^*=5 and Mn=10^{10}. This illustration depicts the correlation between the magnetic field's intensity and its proximity to the current-carrying wire, with a noticeable increase in intensity near the wire. Moreover, the orientation of the magnetic field vectors is consistently directed towards the current-carrying wire.

Fig. 12 displays the effects of MF, and VG and their combined influence on the streamlines, axial velocity profile, secondary flow intensity, and temperature field in the cross-section. Fig. 12 (a) shows two pairs of vortices induced by simply applying an MF. In this way, a pair of large eddies are formed near the wire and another pair on the side of the cross-section. A channel with VG reveals a pair of main vortices, a pair of corner vortices, and two pairs of in-between vortices in the center. Applying an MF and using VG simultaneously shows that some eddies are removed, and some are enhanced due to the interaction between secondary induced flows. The final result is two large eddies in the middle of the cross-
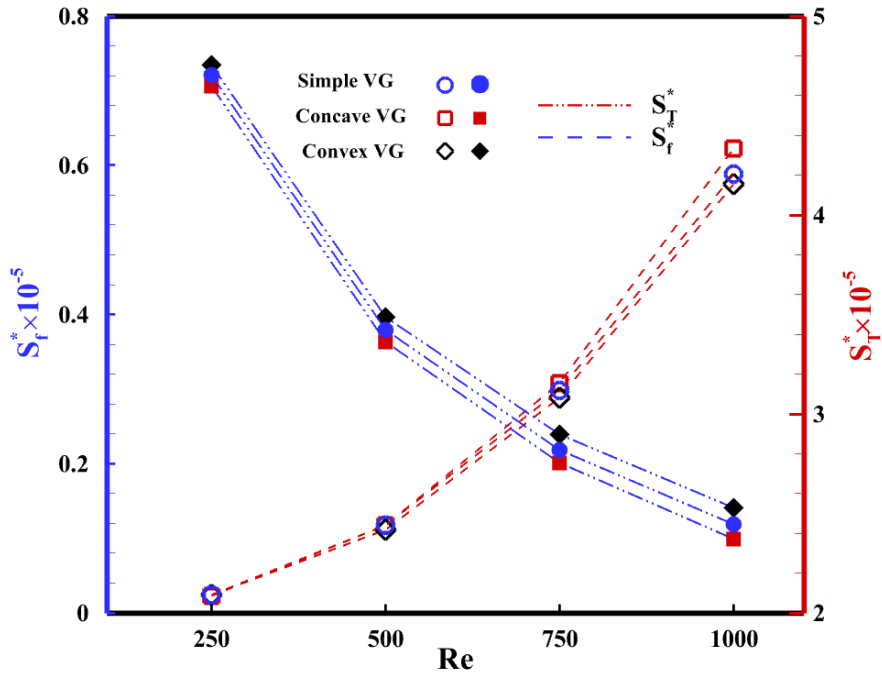
(a)
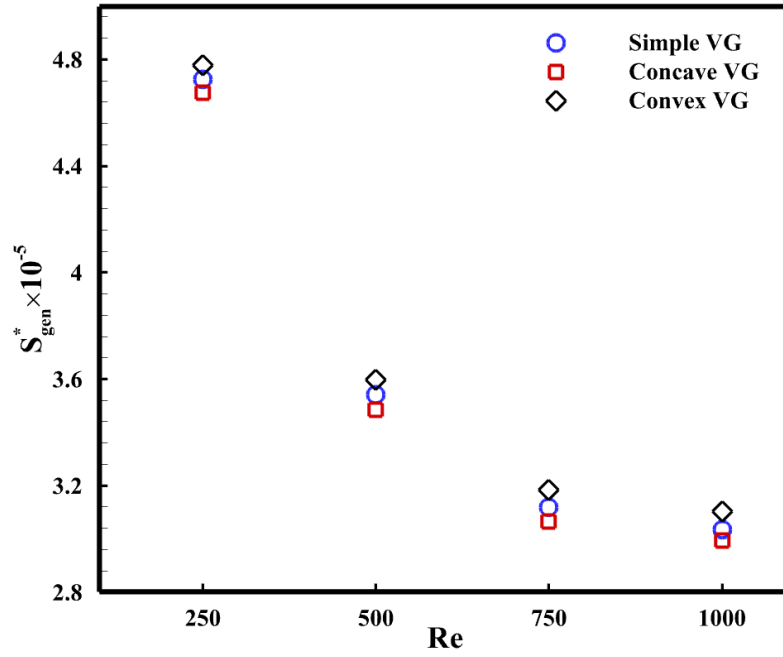
(b)

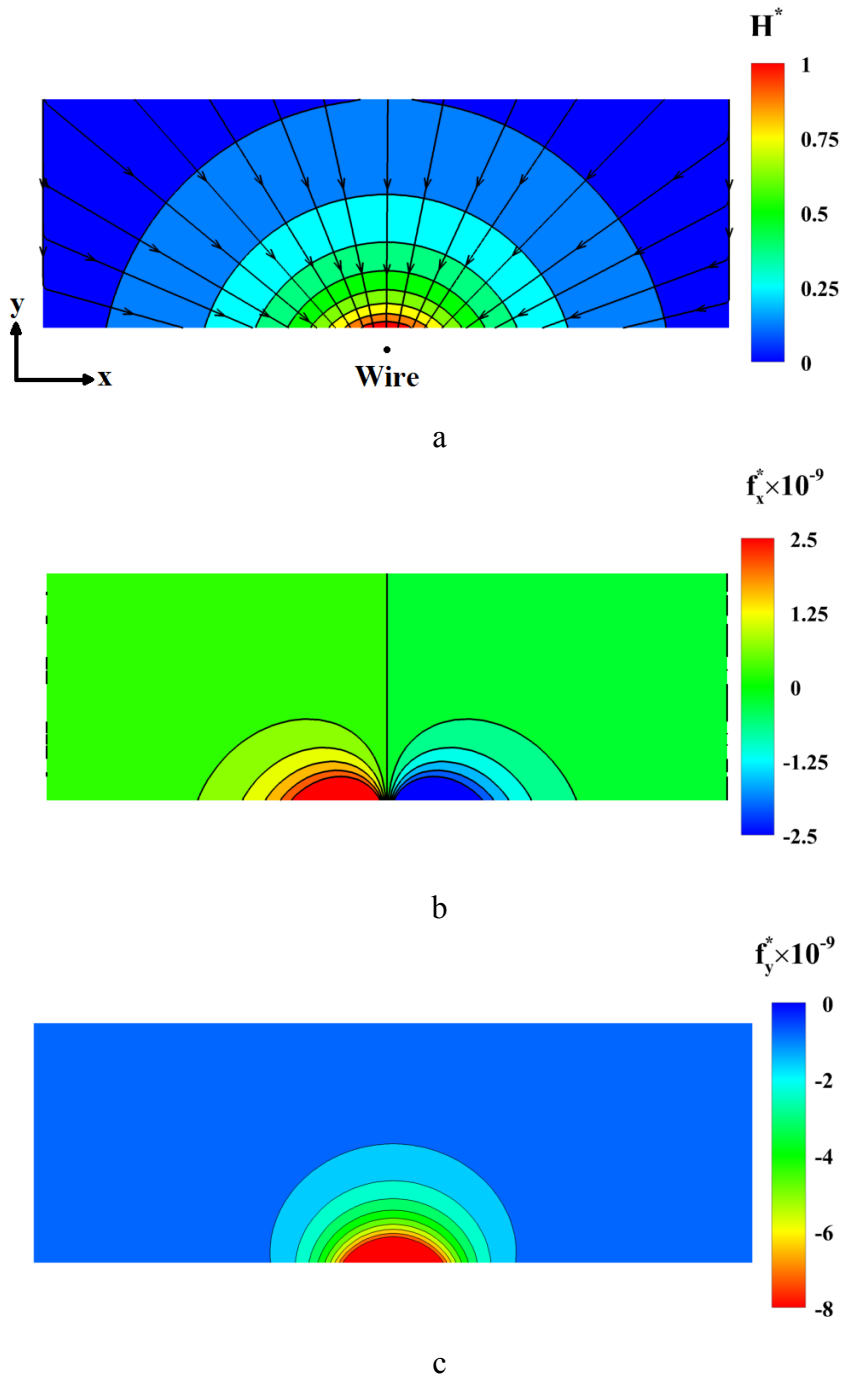**Fig. 10. Variation of a) thermal and frictional entropy and b) total entropy production at Mn=0**

Fig. 11. Distribution of a) MF intensity, b) X component of Kelvin force, and c) Y component of Kelvin force. for and Re=1000
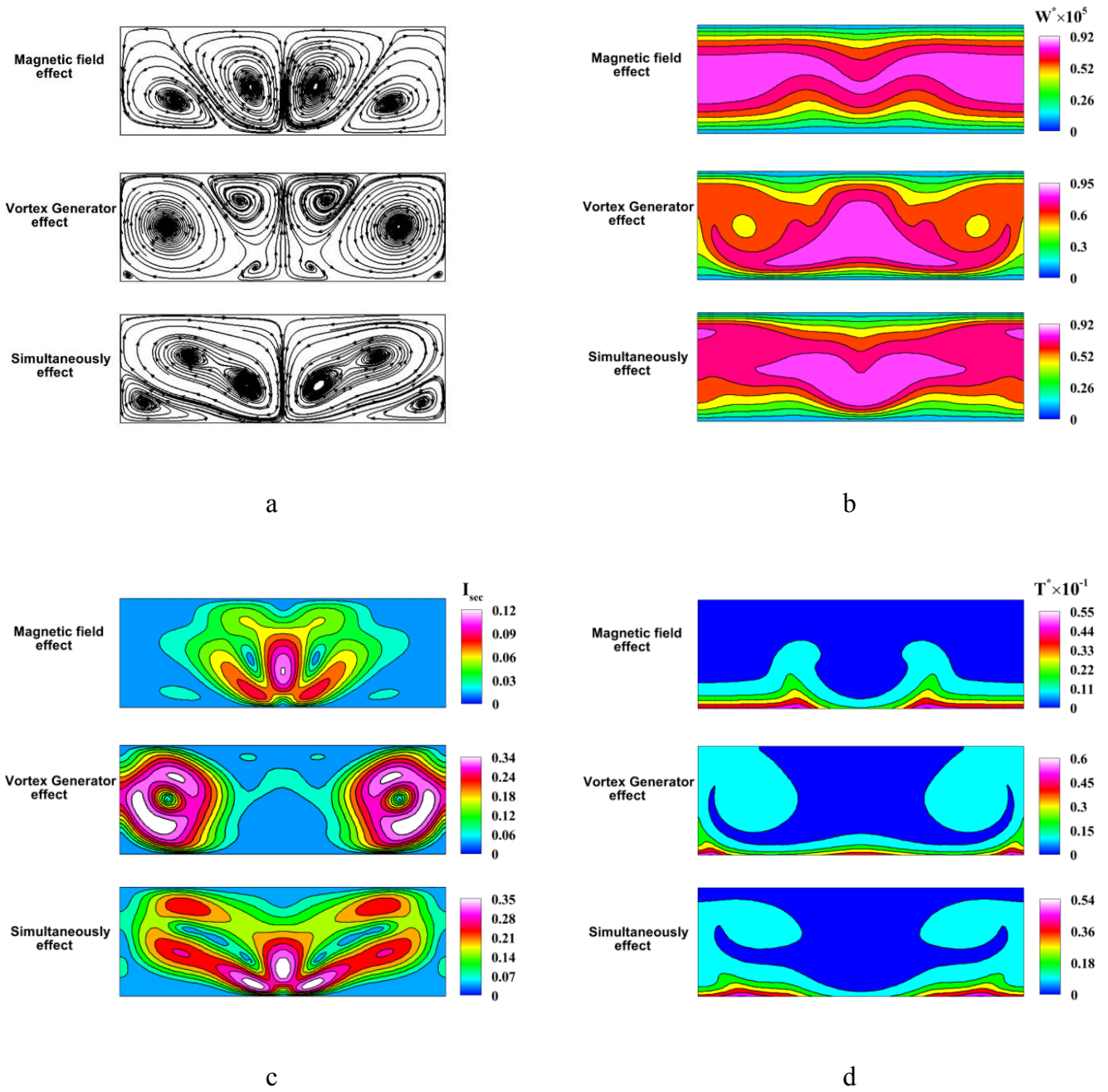
a

b

c

d

Fig. 12. Comparison of the MF, VG and their simultaneous effects on a) streamlines, b) axial velocity, c) secondary flow intensity, and d) temperature field. ($Z^* = 5$, Mn=7.5×10^9 and Re=1000)
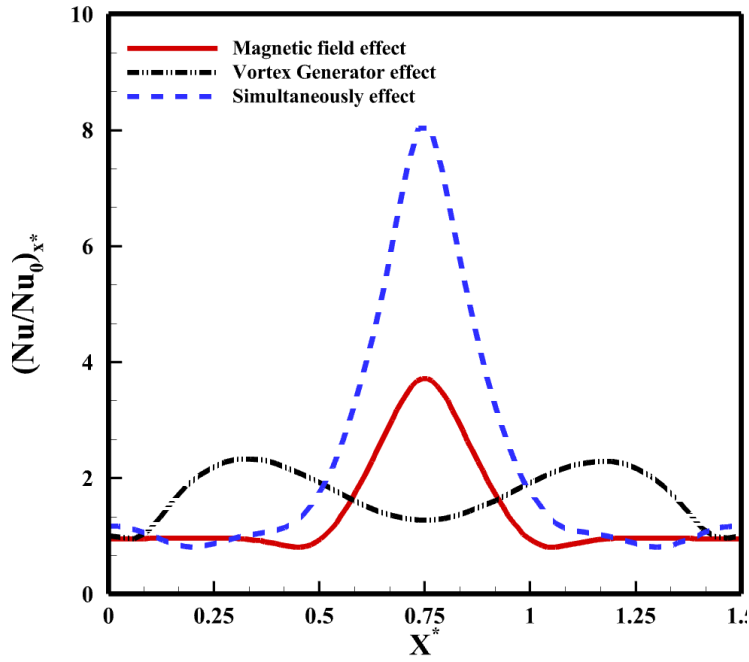
Fig. 13. Variation of the local Nusselt number due to MF, VG, and simultaneous effects at $Mn=7.5\times10^{9}$ **and Re=1000**
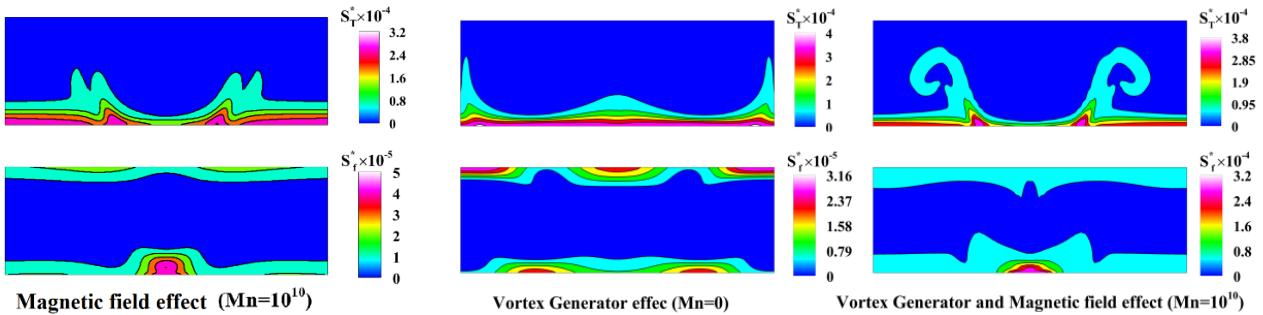

Fig. 14. Comparison of the effect of MF, VG and simultaneous effect on the contours of thermal entropy (top row) and frictional entropy (lower row) at $Mn=7.5\times10^{9}$ **and Re=1000**

section and two smaller ones at the bottom corners. According to Fig.12 (c), by applying a MF, the value of I_{sec} is increased in the vicinity of the MF and by using VG at the sides of the cross-section. Nevertheless, when both the MF and VG are applied simultaneously, the center of the cross-section and the vicinity of the wire exhibit prominent peak values of I_{sec}. Based on Fig. 12 (d), the application of MF increases the mixing strength in the central regions, whereas VG promotes mixing at the sides of the cross-section. When applying MF and VG simultaneously, it can be seen that the MF primarily influences the temperature field within the central regions of the cross-section, whereas the VG exerts a substantial impact on the temperature distribution along the sides of the cross-section.

Fig. 13 indicates the spanwise distribution of the local Nusselt number at $Z^{*}=5$ and $Mn=7.5\times10^{9}$. The figure illustrates that at $x^{*}=0.75$, the local Nusselt number increases by about four times with the application of MF, while this value increases by eight times with the simultaneous application of MF and VG.

The contours of thermal and fluid frictional entropy productions under the action of MF, VG, and the simultaneous application of both are shown in Fig. 14. The figure demonstrates that significant amounts of entropy are generated due to friction near walls with strong velocity gradients. The highest irreversibility occurs near the bottom wall, subject to external heat flux. Applying MF or VG increases heat transfer and reduces the temperature gradient,
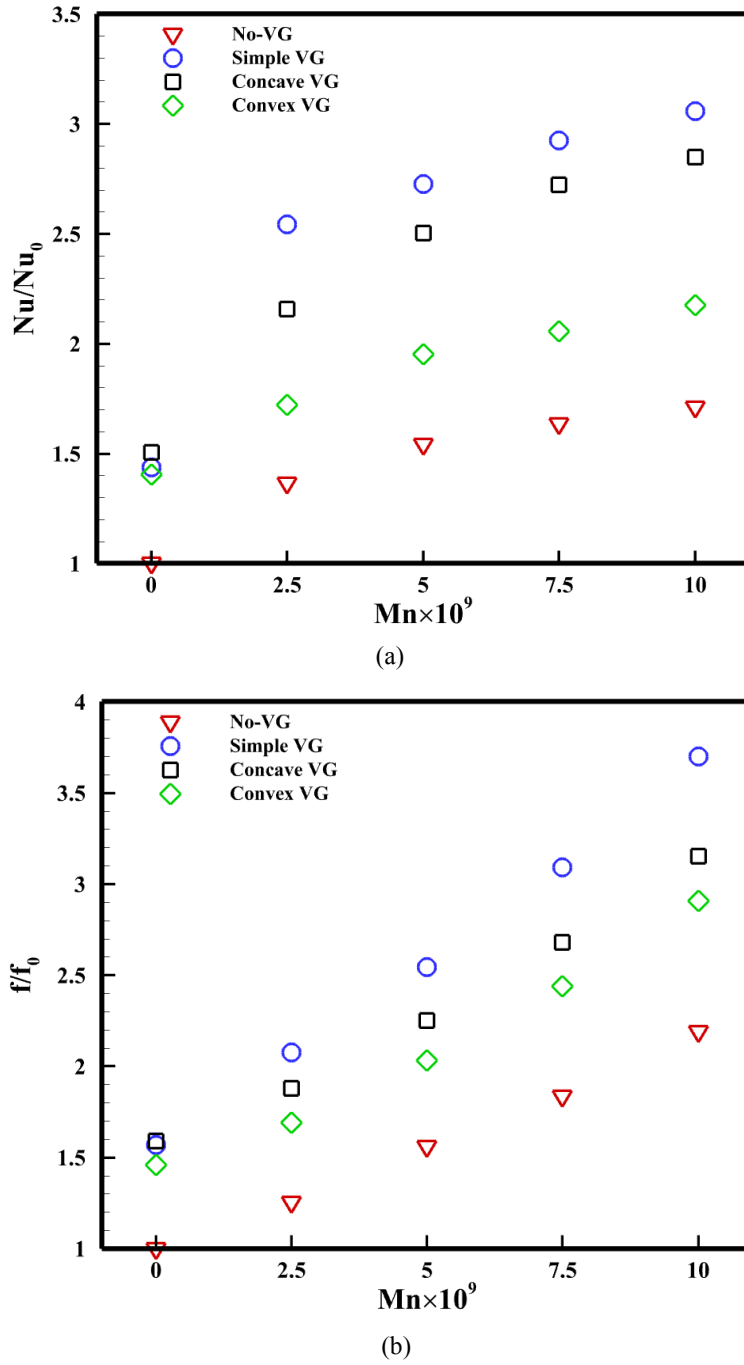
(a)

(b)

Fig. 15. Variation of a) average Nusselt number, b) pressure drop coefficient, and c) thermal performance coefficient according to the VG types at Re=1000 (Continued)

resulting in significantly reduced thermal entropy generation compared to the channel without VG and MF.

Fig.15 depicts the variation of the Nu/Nu_0, f/f_0, and PEC for the three types of VGs. Referring to Fig. 15 (a) and (b), there is an increase in both the Nusselt number and pressure drop coefficient when VG and MF are present. When the MF is not present but the VG is, it is observed that the channels with concave VG profiles exhibit the highest values for Nu/Nu_0 and f/f_0, reaching 1.50 and 1.59, respectively. On the other hand, when a MF of $Mn=10^{10}$ is applied to the channel without VG, the values of Nu/Nu_0 and f/f_0 are 1.71 and 2.19, respectively. By comparing the values of Nu/Nu_0 and f/f_0, to attain a certain level of heat transfer enhancement, the MF results in a greater pressure drop. In the presence of
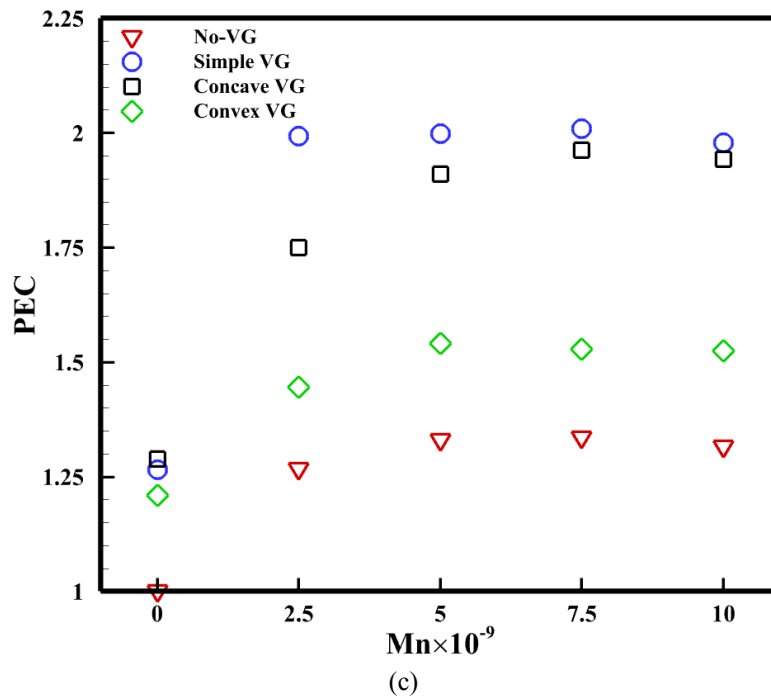
Fig. 15. Variation of a) average Nusselt number, b) pressure drop coefficient, and c) thermal performance coefficient according to the VG types at Re=1000.

an MF, the simple VG exhibits a higher Nusselt number and pressure drop coefficient than the other two VGs. Based on the figure, it is evident that the channel has a concave VG, and under the influence of an MF of $Mn=10^{10}$, the values of Nu/Nu_0 and f/f_0 are 2.85 and 3.15, respectively. These results indicate that when MF and VG are presented together, there is a 185% enhancement in the Nusselt number and a 215% increase in the pressure drop coefficient. The application of MF and VG alone increased the heat transfer by 50% and 71%, respectively, but the combined effect resulted in a notable increase of 185% in the Nusselt value. According to Fig. 15 (c), it is evident that the channel with a concave VG has the greatest PEC, with a value of 1.288 in the absence of MF. Furthermore, the maximum PEC in the presence of MF (with a strength of $Mn=7.5\times10^9$) is obtained in the channel without VG, with a value of 1.335. By applying MF and a concave VG simultaneously, the highest PEC is obtained for a magnetic number of $Mn=7.5\times10^9$ with a value of 1.96.

Comparing the irreversibility levels of the three types of VG is illustrated in Fig.16. In the absence of MF, the channel with a concave VG has the highest production of frictional entropy and the lowest heat transfer irreversibility according

to Fig. 16 (a). However, in the presence of MF, these conditions can be observed in a channel with a simple VG. According to Fig. 16 (b), the minimum overall entropy is generated for the simple, concave, and convex VGs at $Mn=2.5\times10^9$. In accordance with the second law of thermodynamics, the optimal operating condition is a channel with a convex VG at a magnetic number of $Mn=2.5\times10^9$.

According to the results obtained in the previous sections, the optimal operating condition is specified in Table 6.

9- Conclusions

In this paper, the convection heat transfers and flow specifications of ferrofluid in a 3D rectangular channel have been simulated. A combined technique involving the simultaneous use of a rectangular winglet-type vortex generator and an MF has been utilized to intensify the heat transfer rate. It examines how Reynolds number, vortex generator type, and magnetic number affect heat transfer rate, flow losses, thermal performance, and entropy production. Some of the significant findings of this paper are:

• VGs have a more pronounced role in improving the
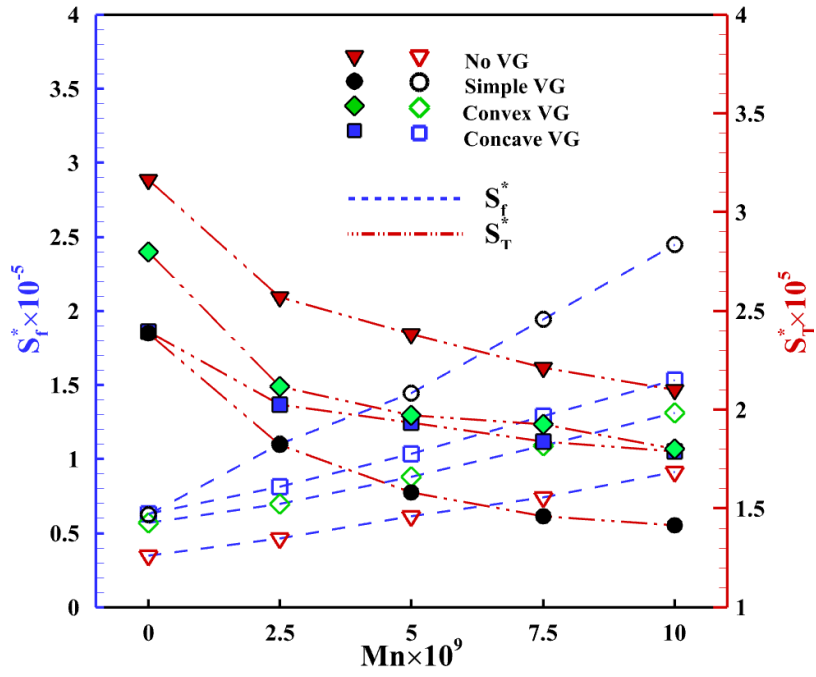
(a)
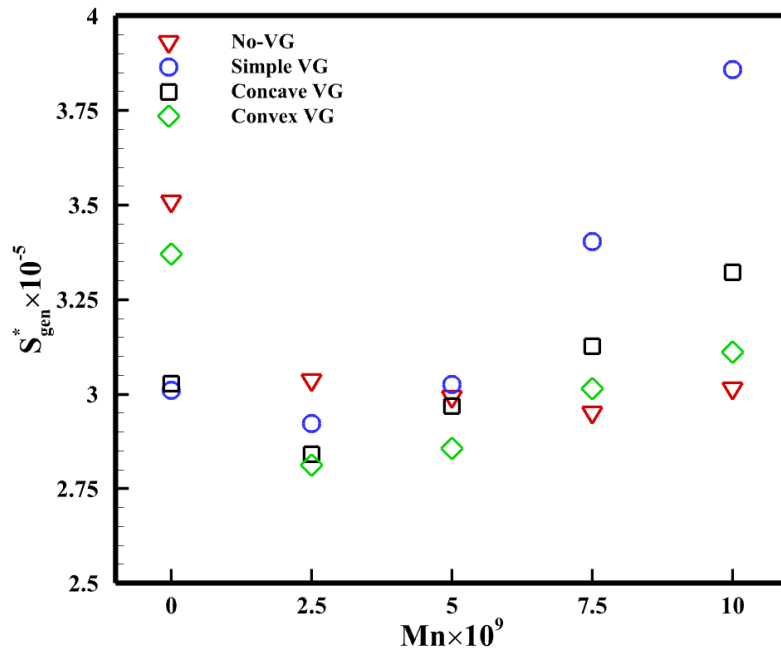
(b)

Fig. 16. Variation of the a) frictional and thermal entropy production and b) total entropy production.

Table 5. Comparison of the Nusselt number in a channel with rectangular VG with the experimental study [46]

			Mn (×E+09)	Re	VG Type	f/f0	Nu/Nu0	PEC	S*(×E-5)
Optimal	**Simple Channel**	**Mn≠0**	7.5	1000	-	1.8	1.6	1.33	2.95
	Vortex Generator	**Mn=0**	-	1000	Concave VG	1.6	1.5	1.28	3
		Mn≠0	7.5	1000	Simple VG	3.1	2.7	2	3.4

convection rate at high Reynolds numbers.
- Among the three VGs investigated, the concave VG yielded the highest Nu/Nu_0, f/f_0, and PEC values and the lowest total entropy generation rate when Mn=0.
- Using vortex generators in the absence of the magnetic field increases heat transfer rate and pressure drop by 50% and 60%, respectively.
- Comparison of Nu/Nu_0 and f/f_0 values in channel a without VG leads to the conclusion that MF results in a higher-pressure drop compared to a channel with VG when Mn=0.
- MF and VG separately intensify the heat transfer rate by 70% and 50%, respectively, whereas their simultaneous effect results in a Nusselt number augmentation of 200%.
- MF and VG separately augment the pressure drop by 118% and 60%, respectively, whereas their simultaneous effect results in a pressure drop augmentation of 269%.
- In the presence of MF, the channel with a convex VG has the lowest entropy production rate at $Mn=2.5×10^9$.
- In the absence of MF, the minimum entropy is generated in a channel having a concave VG. On the contrary, from a thermodynamics point of view, the convex VG performs the most efficiently in the presence of MF.

Nomenclature

D_h	Hydraulic diameter (m)
Ec	Eckert number (-)
f	Fanning friction factor (-)
H	Magnetic field intensity (A/m)
I_{sec}	Secondary flow intensity (-)
k	Thermal conductivity (W/m.K)
k_B	Boltzmann coefficient (J/K)
Mn	Magnetic number (-)
Nu	Average Nusselt number (-)
P^*	Non-dimensional pressure (-)
Pe	Peclet number (-)
PEC	Thermal performance coefficient (-)
Pr	Prandtl number (-)
q^*	Non-dimensional heat flux (-)
Re	Reynolds number (-)

S^*	Non-dimensional entropy generation (-)
T^*	Non-dimensional temperature (-)

Greek symbols

ρ	Density (Kg/m^3)
φ	Nano particle volume fraction (-)
ζ	Langevin parameter (-)
μ	Dynamic viscosity (Pa.s)
$μ_0$	Permeability of free space (Tm/A)

Subscripts/superscripts

bf	Base fluid
ff	ferrofluid
gen	generation
np	Nanoparticle
p	particle
0	Reference state
w	wall

References

[1] F.L. Rashid, A.K. Hussein, E.H. Malekshah, A. Abderrahmane, K. Guedri, O. Younis, Review of Heat Transfer Analysis in Different Cavity Geometries with and without Nanofluids, Nanomaterials, 12(14) (2022) 2481.

[2] M.T. Al-Asadi, H.A. Mohammed, M.C. Wilson, Heat Transfer Characteristics of Conventional Fluids and Nanofluids in Micro-Channels with Vortex Generators: A Review, Energies, 15(3) (2022) 1245.

[3] S. Caliskan, S. Şevik, Ö. Özdilli, Heat transfer enhancement by a sinusoidal wavy plate having punched triangular vortex generators, International Journal of Thermal Sciences, 181 (2022) 107769.

[4] A.J. Modi, M.K. Rathod, Experimental investigation of heat transfer enhancement and pressure drop of fin-and-circular tube heat exchangers with modified rectangular winglet vortex generator, International Journal of Heat and Mass Transfer, 189 (2022) 122742.

[5] H. Soltanipour, F. Pourfattah, Simultaneous use of non-uniform magnetic field and porous medium for the

intensification of convection heat transfer of a magnetic nanofluid inside a tube, Journal of the Brazilian Society of Mechanical Sciences and Engineering, 43 (2021) 1-19.

[6] S.M. Mousavi, M. Biglarian, A.A.R. Darzi, M. Farhadi, H.H. Afrouzi, D. Toghraie, Heat transfer enhancement of ferrofluid flow within a wavy channel by applying a non-uniform magnetic field, Journal of Thermal Analysis and Calorimetry, 139 (2020) 3331-3343.

[7] M. Ibrahim, T. Saeed, F.R. Bani, S.N. Sedeh, Y.-M. Chu, D. Toghraie, Two-phase analysis of heat transfer and entropy generation of water-based magnetite nanofluid flow in a circular microtube with twisted porous blocks under a uniform magnetic field, Powder Technology, 384 (2021) 522-541.

[8] A. Rezaei Gorjaei, F. Joda, R. Haghighi Khoshkhoo, Heat transfer and entropy generation of water–Fe $_3$ O $_4$ nanofluid under magnetic field by Euler–Lagrange method, Journal of Thermal Analysis and Calorimetry, 139 (2020) 2023-2034.

[9] A. Izadi, M. Siavashi, H. Rasam, Q. Xiong, MHD enhanced nanofluid mediated heat transfer in porous metal for CPU cooling, Applied Thermal Engineering, 168 (2020) 114843.

[10] M. Bezaatpour, H. Rostamzadeh, Heat transfer enhancement of a fin-and-tube compact heat exchanger by employing magnetite ferrofluid flow and an external magnetic field, Applied Thermal Engineering, 164 (2020) 114462.

[11] H. Bian, K. Ali, S. Ahmad, H. Bashir, W. Jamshed, K. Irshad, M.K. Al Mesfer, M. Danish, S.M. El Din, Interaction of micro-fluid structure in a pressure-driven duct flow with a nearby placed current-carrying wire: A numerical investigation, Reviews on Advanced Materials Science, 62(1) (2023) 20230134.

[12] B. Sun, Y. Guo, D. Yang, H. Li, The effect of constant magnetic field on convective heat transfer of Fe3O4/water magnetic nanofluid in horizontal circular tubes, Applied Thermal Engineering, 171 (2020) 114920.

[13] H. Roshani, P. Jalili, B. Jalili, I. Ahmad, A.S. Hendy, M.R. Ali, D. Ganji, The effect of magnetic field on the heat transfer in the porous medium octagonal cavity with Cassini oval barriers, Case Studies in Thermal Engineering, 56 (2024) 104194.

[14] Z. Mehrez, A. El Cafsi, Heat exchange enhancement of ferrofluid flow into rectangular channel in the presence of a magnetic field, Applied Mathematics and Computation, 391 (2021) 125634.

[15] F. Selimefendigil, H.F. Öztop, Effects of local curvature and magnetic field on forced convection in a layered partly porous channel with area expansion, International Journal of Mechanical Sciences, 179 (2020) 105696.

[16] H. Soltanipour, Two-phase simulation of magnetic field effect on the ferrofluid forced convection in a pipe considering Brownian diffusion, thermophoresis, and magnetophoresis, The European Physical Journal Plus, 135(9) (2020) 1-23.

[17] H.Z. Demirag, M. Dogan, A.A. Igci, The numerical analysis of novel type conic vortex generator and comparison with known VGs for heat transfer enhancement, Heat and Mass Transfer, (2022) 1-28.

[18] D. Hu, Q. Zhang, K. Song, C. Gao, K. Zhang, M. Su, L. Wang, Performance optimization of a wavy finned-tube heat exchanger with staggered curved vortex generators, International Journal of Thermal Sciences, 183 (2023) 107830.

[19] L. Yang, L. Shi, X. Ding, W. Cui, G. Chang, C. Wang, G. Yue, Y. Li, Numerical analysis of the performance of proton exchange membrane fuel cell with longitudinal vortex generators, Energy Reports, 8 (2022) 9481-9492.

[20] C. Xie, G. Yan, Q. Ma, Y. Elmasry, P.K. Singh, A. Algelany, M. Wae-hayee, Flow and heat transfer optimization of a fin-tube heat exchanger with vortex generators using Response Surface Methodology and Artificial Neural Network, Case Studies in Thermal Engineering, 39 (2022) 102445.

[21] Z. Ke, C.-L. Chen, K. Li, S. Wang, C.-H. Chen, Vortex dynamics and heat transfer of longitudinal vortex generators in a rectangular channel, International Journal of Heat and Mass Transfer, 132 (2019) 871-885.

[22] Y. Amini, S. Akhavan, E. Izadpanah, A numerical investigation on the heat transfer characteristics of nanofluid flow in a three-dimensional microchannel with harmonic rotating vortex generators, Journal of Thermal Analysis and Calorimetry, 139 (2020) 755-764.

[23] A. Heydari, A. Noori, A.K. Nezhad, K. Kord, Optimized heat transfer systems: Exploring the synergy of micro pin-fins and micro Vortex generators, International Communications in Heat and Mass Transfer, 153 (2024) 107378.

[24] S. Asaadi, H. Abdi, Numerical investigation of laminar flow and heat transfer in a channel using combined nanofluids and novel longitudinal vortex generators, Journal of Thermal Analysis and Calorimetry, 145 (2021) 2795-2808.

[25] T. Lemenand, C. Habchi, D. Della Valle, H. Peerhossaini, Vorticity and convective heat transfer downstream of a vortex generator, International Journal of Thermal Sciences, 125 (2018) 342-349.

[26] Z. Li, D. Lu, Q. Cao, Y. Wang, Y. Liu, Research on the enhanced heat transfer performance of SCO2 caused by vortex generators with different geometric dimensions in novel airfoil channels, Progress in Nuclear Energy, 169 (2024) 105057.

[27] E. Tzirtzilakis, M. Xenos, Biomagnetic fluid flow in a driven cavity, Meccanica, 48 (2013) 187-200.

[28] H. Soltanipour, Numerical analysis of two-phase ferrofluid forced convection in an annulus subjected to magnetic sources, Applied Thermal Engineering, 196 (2021) 117278.

[29] R.E. Rosensweig, Heating magnetic fluid with alternating magnetic field, Journal of magnetism and magnetic materials, 252 (2002) 370-374.

[30] A. Gavili, F. Zabihi, T.D. Isfahani, J. Sabbaghzadeh, The thermal conductivity of water base ferrofluids under magnetic field, Experimental Thermal and Fluid Science, 41 (2012) 94-98.

[31] B.C. Pak, Y.I. Cho, Hydrodynamic and heat transfer study of dispersed fluids with submicron metallic oxide

particles, Experimental Heat Transfer an International Journal, 11(2) (1998) 151-170.

[32] A. Karimi, M. Goharkhah, M. Ashjaee, M.B. Shafii, Thermal Conductivity of Fe _ 2 O _ 3 Fe 2 O 3 and Fe _ 3 O _ 4 Fe 3 O 4 Magnetic Nanofluids Under the Influence of Magnetic Field, International Journal of Thermophysics, 36 (2015) 2720-2739.

[33] L. Wang, Y. Wang, X. Yan, X. Wang, B. Feng, Investigation on viscosity of Fe3O4 nanofluid under magnetic field, International Communications in Heat and Mass Transfer, 72 (2016) 23-28.

[34] F.P. Incropera, D.P. DeWitt, T.L. Bergman, A.S. Lavine, Fundamentals of heat and mass transfer, Wiley New York, 1996.

[35] L.S. Sundar, M. Naik, K. Sharma, M. Singh, T.C.S. Reddy, Experimental investigation of forced convection heat transfer and friction factor in a tube with Fe3O4 magnetic nanofluid, Experimental Thermal and Fluid Science, 37 (2012) 65-71.

[36] S.Y. Motlagh, H. Soltanipour, Natural convection of Al2O3-water nanofluid in an inclined cavity using Buongiorno's two-phase model, International Journal of Thermal Sciences, 111 (2017) 310-320.

[37] D. Pnueli, Principles of enhanced heat transfer: by RL Webb. Wiley-Interscience, New York (1994), in, Pergamon, 1995.

[38] A. Bejan, Second-law analysis in heat transfer and thermal design, in: Advances in heat transfer, Elsevier, 1982, pp. 1-58.

[39] A. Bejan, Entropy generation minimization: The new thermodynamics of finite-size devices and finite-time processes, Journal of Applied Physics, 79(3) (1996) 1191-1218.

[40] A. Bejan, J. Kestin, Entropy generation through heat and fluid flow, (1983).

[41] N. Hajialigol, A. Fattahi, M.H. Ahmadi, M.E. Qomi, E. Kakoli, MHD mixed convection and entropy generation in a 3-D microchannel using Al2O3–water nanofluid, Journal of the Taiwan Institute of Chemical Engineers, 46 (2015) 30-42.

[42] S.V. Patankar, Heat conduction, Numerical heat transfer and fluid flow, (2018) 41-77.

[43] M. Asfer, B. Mehta, A. Kumar, S. Khandekar, P.K. Panigrahi, Effect of magnetic field on laminar convective heat transfer characteristics of ferrofluid flowing through a circular stainless steel tube, International Journal of Heat and Fluid Flow, 59 (2016) 74-86.

[44] H. Aminfar, M. Mohammadpourfard, S.A. Zonouzi, Numerical study of the ferrofluid flow and heat transfer through a rectangular duct in the presence of a non-uniform transverse magnetic field, Journal of Magnetism and Magnetic materials, 327 (2013) 31-42.

[45] M.H. Hekmat, K.K. Ziarati, Effects of nanoparticles volume fraction and magnetic field gradient on the mixed convection of a ferrofluid in the annulus between vertical concentric cylinders, Applied Thermal Engineering, 152 (2019) 844-857.

[46] G. Zhou, Q. Ye, Experimental investigations of thermal and flow characteristics of curved trapezoidal winglet type vortex generators, Applied Thermal Engineering, 37 (2012) 241-248.

[47] A. Abdollahi, M. Shams, Optimization of shape and angle of attack of winglet vortex generator in a rectangular channel for heat transfer enhancement, Applied Thermal Engineering, 81 (2015) 376-387.